Generation of multimode squeeze operators and multipartite entangled states for continuous variables

Hong Sun[*]

State Key Laboratory of Modern Optical Instrumentation, Department of Optical Engineering, Zhejiang University, Hangzhou 310027, China

A scheme is presented for generating unitarily multimode field squeezing, cluster entanglement, and Greenberger-Horne-Zeilinger (GHZ) entanglement via cavity quantum electrodynamics. Through a suitable laser system, we are able to engineer a squeeze field operator decoupled from the atomic degrees of freedom, yielding a large squeeze parameter proportional to the number of atoms. The physical mechanism is attributed to the multiple four-photon processes and the dispersive atom-cavity-field interaction in large detuning systems.

I. INTRODUCTION

The nonclassical states of light are an amazing topic in quantum optics both theoretically and experimentally [1–3]. They are crucial resources for precision measurements [4] and quantum information processing [5]. Additionally, some squeezed states are simultaneously entangled states [6–8]. It is well known that Lloyd and Braunstein introduced the use of continuous variables (CV) in quantum information [9]. In recent years, increasing attention has been devoted to Gaussian states, as they play a major role in quantum information with CV [5,10–15].

Graph states are multiparty entangled states that correspond to mathematical graphs, where the vertices of the graph take the role of quantum systems and edges represent interactions [16,17]. CV graph states have also been well studied [18,19]. These states include CV Greenberger-Horne-Zeilinger (GHZ) states with applications in quantum communication and CV cluster states, which may serve as a universal resource for quantum computation in the one-way quantum computer [20,21]. There are standard methods of generating continuous-variable cluster states using continuous-variable linear optics [22,23]. Su *et al.* have experimentally produced CV quadripartite cluster and GHZ entangled states [24].

On the other hand, cavity quantum electrodynamics (QED) has been proven to be a promising framework to investigate the foundations of quantum mechanics. For example, Guzmán *et al.* proposed a method to implement single-mode and two-mode field squeeze operators from an atomic cloud in an optical cavity, and they found robust output entanglement can be achieved outside the cavity [25]. However, to our knowledge, effective and tunable multimode squeeze operators are less studied.

In this paper, we present a scheme to realize effective multimode squeezed operators. The resulting multimode squeezed states are highly correlated states of all the cavity modes, exhibiting reduced quadrature noises in linear combinations of variables of all the modes. Meanwhile, they are also CV multipartite entangled states (CV cluster and GHZ entangled states). This provides a possibility to use the QED systems for the one-way quantum computing research.

Here we concentrate on the dispersion interaction. At large detunings, the driving fields and cavity fields are far away from the bare-state atom resonance, and Kerr interaction (dispersion interaction) occurs in the system. The atoms stay in the ground state, and there are only four-photon processes, with no single-photon processes. Using the expression of the dressed atomic state, the cavity modes are far away from the dressed-state resonance, but they are still in the two-photon resonance. This is different from our previous work [26], which addresses the near-resonance system. Both absorption and dispersion are present (both single-photon processes and four-photon processes). Physically, our scheme is based on the quantum interference between multiple wave-mixing interaction channels (Fig. 1). In each channel, two photons are absorbed from the classical driving field, and then two new photons of different frequencies are emitted into the sideband modes [27,28]. Due to parametric conversion, entanglement can arise between the two sidebands [29,30]. Once multiple channels are involved and all the excited states are coupled to the common ground state, quantum interference will take effect. Quantum beats occur between all channels [31–34] and have their effects on both the lower and higher sidebands. This makes the lower and higher sidebands behave as different collective modes and makes them interact with the atoms. As a result, these two collective modes are in a parametric interaction. This determines parametric interactions between any two lower and higher sidebands.

This paper is organized as follows. In Sec. II we obtain multimode squeeze operators in the multiple-channel system. In Sec. III we calculate the variances of the output collective modes to show the two-mode and multimode squeezed states. In Sec. IV we demonstrate that the squeezed states are cluster entangled states. In Sec. V we prove that the squeezed states are GHZ entangled states. Our results are summarized in Sec. VI.

II. MULTIMODE SQUEEZE OPERATORS

We consider an ensemble of N independent atoms in an optical cavity, as shown in Fig. 2. Our model consists of multiple transitions from one common ground state $|0\rangle$ to n excited states $|j\rangle$, $j = 1,2,\ldots,n$, $n \geqslant 1$ (Fig. 1). The transition $|0\rangle - |j\rangle$ is driven by a laser field of circular frequency
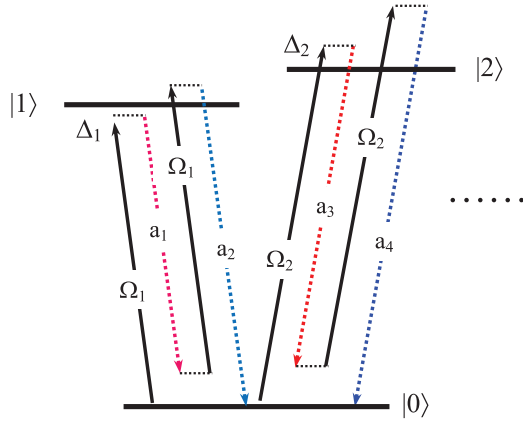
_____
[*]sun_daisy@zju.edu.cn

FIG. 1. (Color online) The multichannel scheme. Each driving field (Rabi frequency Ω_j, $j = 1,2,\ldots,n$, $n \geqslant 1$) drives one transition. In each channel, two photons from the driving field Ω_j are absorbed, and two sideband photons (annihilation operators a_{2j-1} and a_{2j}) are generated.

$\bar{\omega}_j$, with complex Rabi frequency Ω_j. The cavity modes are generated from the lower sidebands with annihilation operators a_{2i-1} ($i = 1,2,\ldots,m$, $m \leqslant n$) and from the higher sidebands with annihilation operators a_{2j}. The noisy effect of spontaneous emission is negligible here for typical values of individual atomic emission rate and in the presence of a large number of atoms. In the rotating-wave approximation and in an appropriate rotating frame, the Hamiltonians involving the driving fields and the cavity fields are, respectively,

$$H_0 = \sum_{j=1}^{n} \sum_{\mu=1}^{N} \hbar \left[\Delta \sigma_{jj}^{\mu} + \frac{\Omega_j}{2} \left(\sigma_{j0}^{\mu} + \sigma_{0j}^{\mu} \right) \right],$$

$$H_I = \sum_{i=1}^{m} \sum_{j=1}^{n} \sum_{\mu=1}^{N} \hbar \left(g_{2i-1} a_{2i-1} e^{-i\delta_1 t} \sigma_{i0}^{\mu} + g_{2j} a_{2j} e^{-i\delta_2 t} \sigma_{j0}^{\mu} \right)$$
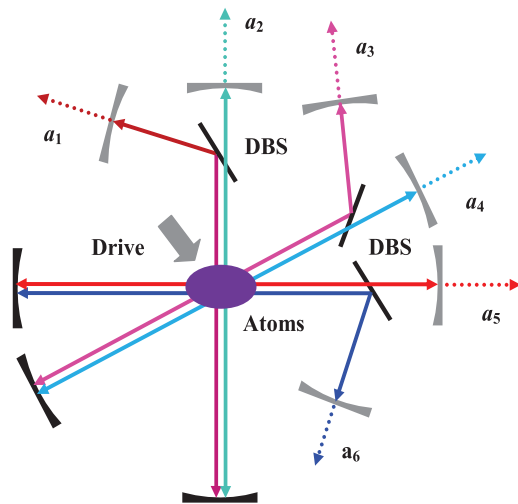
$$+ \text{H.c.} \tag{1}$$

FIG. 2. (Color online) The possible setup for the creation of cluster entanglement and GHZ entanglement of six cavity fields (denoted by the annihilation operators a_{1-6}).

Here H.c. denotes the Hermitian conjugate. In the Hamiltonians, we have assumed that the wave-vector matching is satisfied and the atomic states contain the phase factors due to the randomly oriented moments. For the μ atom, $\sigma_{\alpha\beta}^{\mu} \equiv |\alpha\rangle_{\mu}\langle\beta|$ ($\alpha,\beta = 0,1,2,\ldots,n$) are the atomic spin-flip operators for $\alpha \neq \beta$ and the projection operators for $\alpha = \beta$. $\delta_1 = \omega_{2i-1} - \bar{\omega}_i$ and $\delta_2 = \omega_{2j} - \bar{\omega}_j$ denote the detunings between the sidebands and the corresponding driving fields, where ω_{2i-1} and ω_{2j} are the circular frequencies of fields a_{2i-1} and a_{2j}, respectively. We assume equal atom-driving-field detuning $\Delta = \omega_{j0} - \bar{\omega}_j$, with ω_{j0} being the transition frequencies between levels $|0\rangle$ and $|j\rangle$. g_{2i-1} (g_{2j}) denote the complex coupling strengths of cavity fields a_{2i-1} (a_{2j}) with the atoms.

(i) *Quantum beats*. First, we introduce the superposition states of the atomic excited states as follows:

$$|\tilde{j}\rangle = \sum_{k=1}^{n} U_{jk}^{n}|k\rangle, \quad j,k = 1,2,\ldots,n, \tag{2}$$

where $U_{jk}^{n} = (U^n)_{jk}$,

$$U^2 = \begin{pmatrix} c_1 & s_1 \\ -s_1 & c_1 \end{pmatrix}, \quad U^3 = \begin{pmatrix} c_1 c_2 & s_1 c_2 & s_2 \\ -s_1 & c_1 & 0 \\ -c_1 s_2 & -s_1 s_2 & c_2 \end{pmatrix},$$

$$U^4 = \begin{pmatrix} c_1 c_2 c_3 & s_1 c_2 c_3 & s_2 c_3 & s_3 \\ -s_1 & c_1 & 0 & 0 \\ -c_1 s_2 & -s_1 s_2 & c_2 & 0 \\ -c_1 c_2 s_3 & -s_1 c_2 s_3 & -s_2 s_3 & c_3 \end{pmatrix}, \ldots, \tag{3}$$

with $s_l = \frac{\Omega_{l+1} e^{-i\phi_1}}{\Omega}$, $c_l = \sqrt{1 - |s_l|^2}$, $l = 1,2,\ldots,n-1$, $\phi_1 = \arg \Omega_1$, and $\Omega = \sqrt{\sum_{j=1}^{n} |\Omega_j|^2}$. Then the Hamiltonian H_0 can be rewritten as

$$H_0 = \sum_{\mu=1}^{N} \hbar \left[\Delta \sigma_{\tilde{1}\tilde{1}}^{\mu} + \frac{\Omega}{2} \left(\sigma_{\tilde{1}0}^{\mu} e^{i\phi_1} + \sigma_{0\tilde{1}}^{\mu} e^{-i\phi_1} \right) \right]. \tag{4}$$

Equation (4) shows that only superposition state $|\tilde{1}\rangle$ is coupled to the driving fields with Rabi frequency Ω, while the other superposition states $|\tilde{j}\rangle$ ($j = 2,3,4,\ldots$) are decoupled and not excited. This results from the multiple quantum interference.

(ii) *Dressed atomic states*. We introduce the basis of the dressed atomic states. This is preferable when the driving fields are strong ($\bar{\Omega} = \sqrt{\Delta^2 + \Omega^2} \gg \gamma$). The Hamiltonian H_0 can be easily diagonalized to show the interactions of the sidebands with the atoms. The eigenvectors $|\pm\rangle$ are mixtures of the bare atomic state $|0\rangle$ and superposition state $|\tilde{1}\rangle$ and are known as dressed states [35]:

$$|+\rangle = c|\tilde{1}\rangle + s|0\rangle, \quad |-\rangle = -s|\tilde{1}\rangle + c|0\rangle, \tag{5}$$

with $s = e^{i\phi_1}\sqrt{(1 - \Delta/\bar{\Omega})/2}$ and $c = \sqrt{1 - |s|^2}$; the corresponding eigenvalues are $\lambda_{\pm} = (\Delta \pm \bar{\Omega})/2$, respectively. Then we can rewrite H_0 as $H_0 = \sum_{\mu=1}^{N} \hbar(\lambda_+ \sigma_{++}^{\mu} + \lambda_- \sigma_{--}^{\mu})$. We assume the atoms stay initially in the ground state $|0\rangle$. In terms of the dressed states, the atoms remain in $|-\rangle$ for $\Delta \gg |\Omega|$ or in $|+\rangle$ for $-\Delta \gg |\Omega|$.

(iii) *Collective fields*. The collective modes are [33]

$$A_{2i-1} = \sum_{k=1}^{m} \tilde{U}_{ik}^m a_{2k-1}, \quad A_{2j} = \sum_{k'=1}^{n} \bar{U}_{jk'}^n a_{2k'}, \qquad (6)$$

where we use the index m to allow the number of the odd modes to be less than that of the even modes, $m \leqslant n$. The unitary transform matrix $\tilde{U}^m$ ($\bar{U}^n$) takes exactly the same form as U^m (U^n) except for the substitutions of $\tilde{s}_l$ and $\tilde{c}_l$ for s_l and c_l, respectively, $l = 1, 2, \ldots, m-1$ $(n-1)$. Here $\tilde{s}_l = g_{2l+1} s_l e^{-i\theta_1}/|\tilde{g}_1|$ ($\tilde{s}_l = g_{2l+2} s_l e^{-i\theta_2}/|\tilde{g}_2|$), $\tilde{c}_l = \sqrt{1 - |\tilde{s}_l|^2}$, and the effective coupling strengths are

$$\tilde{g}_1 = e^{i\theta_1} \sqrt{\sum_{i=1}^{m} |g_{2i-1} U_{1i}^m|^2}, \quad \tilde{g}_2 = e^{i\theta_2} \sqrt{\sum_{j=1}^{n} |g_{2j} U_{1j}^n|^2}, \qquad (7)$$

with $\theta_{1,2} = \arg g_{1,2}$, respectively. Only collective modes A_1 and A_2 interact with the dressed transition $|+\rangle \leftrightarrow |-\rangle$, while the other collective modes, A_{2i-1} and A_{2j} $(i, j \geqslant 2)$, are decoupled. These are the very effects of the quantum beats [33]. The uncoupled collective modes A_{2i-1} and A_{2j} $(i, j \geqslant 2)$ remain at their vacuum states. Hence, the Hamiltonian only relates to the atomic transition $|+\rangle \leftrightarrow |-\rangle$ and the collective fields $A_{1,2}$.

(iv) *Effective Hamiltonian*. At large detunings ($\bar{\Omega} \approx |\Delta|$), we derive the effective Hamiltonian as in [36]. For definiteness we adjust the cavity fields $|\delta_1 + \delta_2| \ll |\delta_{1,2}|$, $(|\Delta|, |\delta_{1,2}|) \gg ||\delta_{1,2}| - |\Delta|| \gg (|\tilde{g}_l \langle A_l \rangle|, \gamma)$ $(l = 1, 2)$. The equation for the density matrix is

$$\dot{\rho} = -\frac{i}{\hbar}[H_I, \rho], \qquad (8)$$

and we have its formal solution $\rho(t) = \rho(0) - \frac{i}{\hbar} \int_0^t dt'[H_I(t'), \rho(t')]$. Substituting this solution back into Eq. (8), we obtain

$$\dot{\rho} = -\frac{i}{\hbar}[H_I(t), \rho(0)] - \frac{1}{\hbar^2} \int_0^t [H_I(t), [H_I(t'), \rho(t')]] dt'. \qquad (9)$$

When $||\delta_{1,2}| - |\Delta|| \gg (|\tilde{g}_l \langle A_l \rangle|, \gamma)$ $(l = 1, 2)$, the first term is fast oscillating compared with the second one and is negligible to a good approximation. Then we can employ a Markovian approximation for the latter. Approximately, the evolution of the density operator is

$$\dot{\rho} = -\frac{i}{\hbar}[H_{\text{eff}}, \rho(t)], \qquad (10)$$

with

$$H_{\text{eff}} = -\frac{i}{\hbar} H_I(t) \int H_I(t') dt', \qquad (11)$$

where the indefinite integral is evaluated at time t without integral constant. We assume $t \gg |\delta_l \pm |\Delta||^{-1}$ and make the secular approximation again. Taking the cavity detunings $|\delta_1 + \delta_2| = \frac{N|\tilde{g}_n|^2}{||\delta_1| - |\Delta||}$, we can remove the dynamical Stark shift and obtain the effective Hamiltonian as

$$H_{\text{eff}} = \hbar(\xi^* A_1 A_2 + \xi A_1^\dagger A_2^\dagger), \qquad (12)$$

where we have defined the coupling coefficient

$$\xi = \frac{|\tilde{g}_1 \tilde{g}_2| N \Omega^2 e^{-i(2\phi_1 + \theta_1 + \theta_2)}}{4\Delta^2(|\Delta| - |\delta_1|)}. \qquad (13)$$

Then we get the unitary two-mode squeeze operator

$$S(z) = \exp(z^* A_1 A_2 - z A_1^\dagger A_2^\dagger), \qquad (14)$$

where $z = i\xi\tau$ is a squeeze parameter that is proportional to the number of atoms N, with τ being the interaction time. This squeeze operator is independent of the atomic degrees of freedom and produces two-mode squeezing on any initial field state. Using Eqs. (6) and (14), we obtain the multimode squeezed operator

$$S_{m+n} = \exp \sum_{i=1}^{m} \sum_{j=1}^{n} (z_{ij}^* a_{2i-1} a_{2j} - z_{ij} a_{2i-1}^\dagger a_{2j}^\dagger), \qquad (15)$$

with $m, n \geqslant 1, n \geqslant m$, and $z_{ij}^* = z^* \tilde{U}_{1i}^m \bar{U}_{1j}^n$.

III. VARIANCES, FLUCTUATIONS, AND SQUEEZING

Now we examine the squeezing properties of the outgoing collective modes. Collective modes A_1 and A_2 are driven by the effective nonlinear interaction in Eq. (14) and by external (axial) laser fields with strengths ε_1 and ε_2, respectively. We assume that each collective mode interacts with an independent heat bath. In the Markov approximation, we can obtain the following coupled Langevin equations:

$$\dot{A}_1 = -i\varepsilon_1^* - \frac{\kappa_1}{2} A_1 + \frac{\xi}{2} A_2^\dagger - \sqrt{\kappa_1} A_1^{\text{in}}(t),$$
$$\dot{A}_2 = -i\varepsilon_2^* - \frac{\kappa_2}{2} A_2 + \frac{\xi}{2} A_1^\dagger - \sqrt{\kappa_2} A_2^{\text{in}}(t), \qquad (16)$$

where $A_l^{\text{in}}(t)$ $(l = 1, 2)$ are annihilation operators of the input fields and κ_l are the cavity decay rates of modes A_l. We have taken $\xi \to i\xi/2$ (with ξ being real) to match standard notation [37]. Then we get the following equations:

$$\delta\dot{A}_1 = -\frac{\kappa_1}{2} \delta A_1 + \frac{\xi}{2} \delta A_2^\dagger - \sqrt{\kappa_1} A_1^{\text{in}}(t),$$
$$\delta\dot{A}_2 = -\frac{\kappa_2}{2} \delta A_2 + \frac{\xi}{2} \delta A_1^\dagger - \sqrt{\kappa_2} A_2^{\text{in}}(t), \qquad (17)$$

where we have used the transforms $A_l = \delta A_l + \bar{\alpha}_l$ $(l = 1, 2)$. $\bar{\alpha}_1 = 2i(\kappa_2 \varepsilon_1^* - \xi\varepsilon_2)/(\xi^2 - \kappa_1\kappa_2)$ and $\bar{\alpha}_2 = 2i(\kappa_1 \varepsilon_2^* - \xi\varepsilon_1)/(\xi^2 - \kappa_1\kappa_2)$ are the steady-state solutions for the collective modes. Now we calculate the solutions of Eq. (17) in the frequency domain:

$$\delta A_1(\omega) = \frac{2\sqrt{\kappa_1}\alpha_2}{\xi^2 - \alpha_1\alpha_2} A_1^{\text{in}}(\omega) + \frac{2\sqrt{\kappa_2}\xi}{\xi^2 - \alpha_1\alpha_2} A_2^{\text{in}\dagger}(-\omega),$$
$$\delta A_2(\omega) = \frac{2\sqrt{\kappa_2}\alpha_1}{\xi^2 - \alpha_1\alpha_2} A_2^{\text{in}}(\omega) + \frac{2\sqrt{\kappa_1}\xi}{\xi^2 - \alpha_1\alpha_2} A_1^{\text{in}\dagger}(-\omega), \qquad (18)$$

where $A(\omega) = \frac{1}{\sqrt{2\pi}} \int_{-\infty}^{\infty} d\tau e^{-i\omega\tau} A(t)$ is the Fourier transform of $A(t)$, with $\alpha_l = \kappa_l - 2i\omega$ $(l = 1, 2)$.

We can express the output fields in terms of the input fields [37]:

$$
A_1^{\text{out}}(\omega) = -\sqrt{\kappa_1}\bar{\alpha}_1\delta(\omega) + \frac{\xi^2 + \alpha_1^*\alpha_2}{\xi^2 - \alpha_1\alpha_2}A_1^{\text{in}}(\omega)
$$
$$
+ \frac{2\xi\sqrt{\kappa_1\kappa_2}}{\xi^2 - \alpha_1\alpha_2}A_2^{\text{in}\dagger}(-\omega),
$$
$$
A_2^{\text{out}}(\omega) = -\sqrt{\kappa_2}\bar{\alpha}_2\delta(\omega) + \frac{\xi^2 + \alpha_1\alpha_2^*}{\xi^2 - \alpha_1\alpha_2}A_2^{\text{in}}(\omega)
$$
$$
+ \frac{2\xi\sqrt{\kappa_1\kappa_2}}{\xi^2 - \alpha_1\alpha_2}A_1^{\text{in}\dagger}(-\omega). \tag{19}
$$

Then we define the two-mode quadrature operators [1,38] as $X = (X_1 + X_2)/2$ and $P = (P_1 + P_2)/2$, where $X_l = (A_l^{\text{out}} + A_l^{\text{out}\dagger})/2$ and $P_l = (A_l^{\text{out}} - A_l^{\text{out}\dagger})/2i$ are the quadrature operators for the output collective modes A_l^{out} ($l = 1,2$). The fluctuations of X and P satisfy the uncertainty relation

$$
\langle\delta X\rangle\langle\delta P\rangle \geqslant \tfrac{1}{8}. \tag{20}
$$

Next, to see the squeezing property explicitly, we compute the variances for the quadrature amplitudes at zero frequency. Using Eq. (19), we can obtain

$$
\langle(\delta X)^2\rangle = \frac{1}{8}\left|\frac{x+1}{x-1}\right|^2, \quad \langle(\delta P)^2\rangle = \frac{1}{8}\left|\frac{x-1}{x+1}\right|^2, \tag{21}
$$

with $\langle(\delta O)^2\rangle \equiv \langle O^2\rangle - \langle O\rangle^2$, $O = X, P$, and $x = \frac{\xi}{\sqrt{\kappa_1\kappa_2}}$ being real. Note that $\langle(\delta X)^2\rangle\langle(\delta P)^2\rangle = 1/64$; it should be a minimum uncertainty field state. If there is no nonlinear coupling, we have $\langle(\delta X)^2\rangle = \langle(\delta P)^2\rangle = 1/8$, which demonstrates that it is a coherent state (including the vacuum state). In general, Eq. (21) indicates that $1/8 \leqslant \langle(\delta X)^2\rangle < \infty$ and $0 \leqslant \langle(\delta P)^2\rangle \leqslant 1/8$. Assuming $\langle(\delta P)^2\rangle = e^{-2r}/8$, we then obtain the reduction parameter $r \equiv 2|z|$ as

$$
r = \ln\left|\frac{x+1}{x-1}\right|. \tag{22}
$$

In principle, if $x = 1$ ($r \to \infty$), the output quadrature P may achieve perfect squeezing $\langle(\delta P)^2\rangle = 0$ at the expense of large fluctuations in the output quadrature X. This two-mode squeezed state is a highly correlated state of the output collective modes A_l^{out} ($l = 1,2$) that exhibits reduced quadrature noise in linear combinations of variables of both modes [39]; however, squeezing is not observed in the fluctuations of each collective mode as follows:

$$
\langle(\delta X_{1,2})^2\rangle = \langle(\delta P_{1,2})^2\rangle = \frac{1}{4} + \frac{2x^2}{(x^2-1)^2},
$$
$$
\langle\delta X_i\delta X_j\rangle = -\langle\delta P_i\delta P_j\rangle = \frac{x(x^2+1)}{(x^2-1)^2}, \tag{23}
$$

where $i,j = 1,2$ and $i \neq j$.

Then we recall the relations

$$
A_1 = \sum_{i=1}^{m}\tilde{U}_{1i}^{m}a_{2i-1}, \quad A_2 = \sum_{j=1}^{n}\bar{U}_{1j}^{n}a_{2j} \tag{24}
$$

and define the quadrature operators $x_l = (a_l^{\text{out}} + a_l^{\text{out}\dagger})/2$ and $p_l = (a_l^{\text{out}} - a_l^{\text{out}\dagger})/2i$ for the output modes a_l^{out} ($l = 1,2,\ldots,2m-1$, and $l = 2m,2m+2,\ldots,2n$). After doing some calculations, we can obtain the multimode quadrature operators and the multimode squeezed state. The resulting multimode squeezed state is the common eigenvector of a set of quadrature combinations. Now we will show it is the cluster state.

IV. CLUSTER ENTANGLEMENT

The cluster-type states are those multimode Gaussian states for which certain quadrature correlations become perfect in the limit of infinite squeezing [22,40],

$$
B - MQ \to 0, \tag{25}
$$

where Q and B denote column vectors of the amplitude and phase quadratures, respectively, for each output mode a_l^{out} ($l = 1,2,\ldots,2m-1$, and $l = 2m,2m+2,\ldots,2n$). M is the adjacency matrix for the graph of a given Gaussian state, which indicates the interactions between different vertices on the graph.

Our cluster states are two-colorable graph states [41,42]. The corresponding two-colorable graphs are given by a set of vertices connected in a specific way by edges: There are two groups of vertices, $\{a_{2i-1}\}$ and $\{a_{2j}\}$ ($i = 1,2,\ldots,m$, $j = 1,2,\ldots,n$), and there are no edges inside either of the groups. The former group is colored red, while the latter is colored blue (Fig. 3). In the ideal case of infinite squeezing, the two-colorable cluster state is a simultaneous zero eigenstate of a set of positions and momenta,

$$
x_{2i-1} - \sum_{k'=1}^{n}x_{2k'} \to 0,
$$
$$
p_{2j} + \sum_{k=1}^{m}p_{2k-1} \to 0. \tag{26}
$$

We use a set of sufficient conditions for the full inseparability of a multimode state [43]. The following inequalities are the criteria for the two-colorable cluster entangled state [22,23]:

$$
Y_C = V_{2i-1,2j}^{C}
$$
$$
= \left\langle\left(\delta x_{2i-1} - \delta x_{2j} - \sum_{k'=1;k'\neq j}^{n}\eta_{2k'}\delta x_{2k'}\right)^2\right\rangle
$$
$$
+ \left\langle\left(\delta p_{2j} + \delta p_{2i-1} + \sum_{k=1;k\neq i}^{m}\eta_{2k-1}\delta p_{2k-1}\right)^2\right\rangle < 1. \tag{27}
$$

The subscript (superscript) C designates the cluster state, $i,k = 1,2,\ldots,m$, $j,k' = 1,2,\ldots,n$, and $\eta_{2k'}$ (η_{2k-1}) are arbitrary
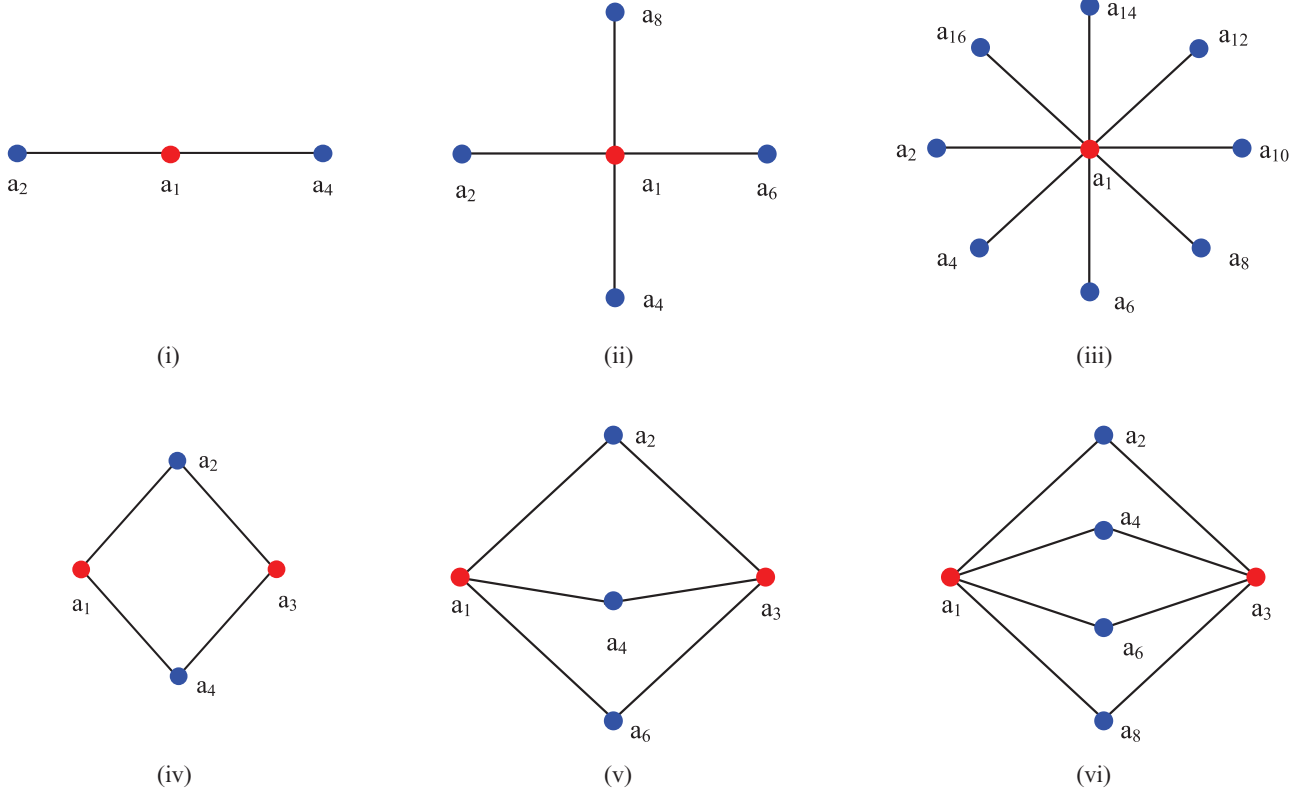
FIG. 3. (Color online) Possible cluster states for different numbers of red sidebands a_{2i-1} and blue sidebands a_{2j}, $i = 1 \sim m$ and $j = 1 \sim n$. For $m = 1$, (i) $n = 2$, (ii) $n = 4$, and (iii) $n = 8$. For $m = 2$, (iv) $n = 2$, (v) $n = 3$, and (vi) $n = 4$. Each vertex takes the role of one mode, and edges represent the interactions between the connected vertices. $\{a_{2i-1}\}$ and $\{a_{2j}\}$ are in two different families.

real parameters that are used to optimize the above inequalities. Calculating the minimum values of the expressions in Eq. (27), we obtain the following linear equations that the optimization parameters should satisfy:

$$
0 = \langle \delta x_{2i-1} \delta x_{2l'} \rangle - \langle \delta x_{2j} \delta x_{2l'} \rangle - \sum_{k'=1; k' \neq j}^{n} \eta_{2k'} \langle \delta x_{2k'} \delta x_{2l'} \rangle,
$$

$$
0 = \langle \delta p_{2j} \delta p_{2l-1} \rangle + \langle \delta p_{2i-1} \delta p_{2l-1} \rangle + \sum_{k=1; k \neq i}^{m} \eta_{2k-1} \langle \delta p_{2k-1} \delta p_{2l-1} \rangle,
$$

(28)

where $l' = 1, 2, \ldots, n$ and $l' \neq j$ ($l = 1, 2, \ldots, m$ and $l \neq i$) for the former (latter) equation. The correlation spectra are written as

$$
Y_C(\omega)\delta(\omega + \omega') = \left\langle \left[\delta x_{2i-1}(\omega) - \delta x_{2j}(\omega) - \sum_{k'=1; k' \neq j}^{n} \eta_{2k'} \delta x_{2k'}(\omega) \right] \left[\delta x_{2i-1}(\omega') - \delta x_{2j}(\omega') - \sum_{k'=1; k' \neq j}^{n} \eta_{2k'} \delta x_{2k'}(\omega') \right] \right\rangle
$$
$$
+ \left\langle \left[\delta p_{2j}(\omega) + \delta p_{2i-1}(\omega) + \sum_{k=1; k \neq i}^{m} \eta_{2k-1} \delta p_{2k-1}(\omega) \right] \left[\delta p_{2j}(\omega') + \delta p_{2i-1}(\omega') + \sum_{k=1; k \neq i}^{m} \eta_{2k-1} \delta p_{2k-1}(\omega') \right] \right\rangle.
$$

(29)

To illustrate the above relation, we consider the particular case

$$
\tilde{U}_{1i}^{m} = \frac{1}{\sqrt{m}}, \quad \bar{U}_{1j}^{n} = \frac{1}{\sqrt{n}},
$$

(30)

with $i = 1, 2, \ldots, m$ and $j = 1, 2, \ldots, n$. This corresponds to the following matching conditions:

$$
g_1 \Omega_1 e^{i(\phi_1 + \theta_1)} = g_{2l+1} \Omega_{l+1} \quad (l = 1, 2, \ldots, m - 1),
$$
$$
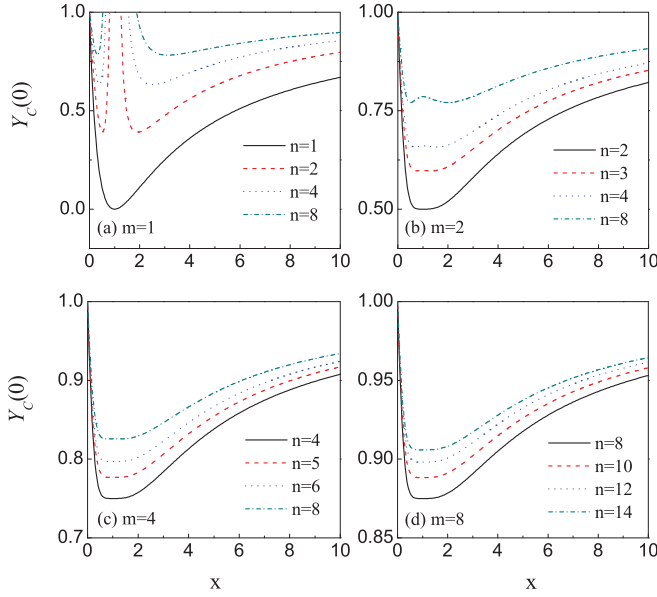g_2 \Omega_1 e^{i(\phi_2 + \theta_2)} = g_{2l+2} \Omega_{l+1} \quad (l = 1, 2, \ldots, n - 1).
$$

(31)

FIG. 4. (Color online) The (dimensionless) output zero-frequency spectra $Y_C(0)$ as functions of x (dimensionless) for different mode numbers m,n.

When $m \geqslant 2$, we have

$$\eta_{2k-1} = \eta_1 = \frac{4\sqrt{\frac{m}{n}}x(x^2+1) - 8x^2}{mx^4 + (6m-8)x^2 + m}. \tag{32}$$

Similarly, for $n \geqslant 2$,

$$\eta_{2k'} = \eta_2 = \frac{4\sqrt{\frac{n}{m}}x(x^2+1) - 8x^2}{nx^4 + (6n-8)x^2 + n}. \tag{33}$$

Letting $h_1 = 1 + (m-1)\eta_1$ and $h_2 = 1 + (n-1)\eta_2$, we obtain

$$Y_C(0) = 1 + \frac{m-1}{4}\eta_1^2 + \frac{n-1}{4}\eta_2^2$$
$$+ \left(\frac{1+h_1^2}{m} + \frac{1+h_2^2}{n}\right)\frac{2x^2}{(x^2-1)^2}$$
$$- \frac{2(h_1+h_2)}{\sqrt{mn}}\frac{x(x^2+1)}{(x^2-1)^2}. \tag{34}$$

When $m = 1$ ($n = 1$), there is no η_{2k-1} ($\eta_{2k'}$), i.e., no η_1 (η_2), and we can also use the above equation to calculate the correlation $Y_C(0)$.

Figure 4 shows numerical results for detecting multimode cluster entanglement. For different mode numbers m and n, we present the output zero-frequency spectra $Y_C(0)$ as functions of x. First, we examine the case of $m = 1$ in Fig. 4(a). If $n = 1$, there is a two-mode state. We should notice that at $x = 1$, the correlation takes the minimum value of zero; that is, this two-mode state exhibits perfect entanglement (Einstein-Podolsky-Rosen entanglement). For $n \geqslant 2$, the spectra bifurcate close to $x = 1$. However, all of them are smaller than 1 over a wide region of $x \neq 1$, which indicates cluster entanglement occurs. With increasing n, $Y_C(0)$ also show an increasing trend.

Next, we plot $Y_C(0)$ for $m = 2$, 4, and 8 to show the scalability of the present scheme. In these cases, the correlation spectra are below unity for $x > 0$. This indicates that the

criteria for the $(m + n)$-mode cluster entangled state are well satisfied. Fixing the value of m and increasing the number of n, $Y_C(0)$ increases successively. When $m = n$, the system is symmetric, and each output zero-frequency spectrum $Y_C(0)$ takes its minimum at $x = 1$. The higher the mode number $(m + n)$ is, the higher the correlation is. But even for the largest mode number ($m = 8$ and $n = 14$), cluster entanglement can exist.

V. GHZ ENTANGLEMENT

Now we examine whether there is CV GHZ entanglement. We consider three types of correlations: each odd mode with each even mode (Y_1), each odd mode with another odd mode (Y_2), and each even mode with another even mode (Y_3). The following inequalities are sufficient to demonstrate CV GHZ entanglement [43]:

$$Y_1 = V_{2i-1,2j}^G = \langle(\delta x_{2i-1} - \delta x_{2j})^2\rangle + \left\langle\left(\left(\delta p_{2i-1} + \delta p_{2j}\right.\right.\right.$$
$$\left.\left.\left. + \sum_{k=1;k\neq i}^m f_{2k-1}\delta p_{2k-1} + \sum_{k'=1;k'\neq j}^n f_{2k'}\delta p_{2k'}\right)^2\right\rangle\right.$$
$$< 1, \tag{35}$$

$$Y_2 = V_{2i_1-1,2i_2-1}^G = \langle(\delta x_{2i_1-1} - \delta x_{2i_2-1})^2\rangle + \left\langle\left(\left(\delta p_{2i_1-1}\right.\right.\right.$$
$$\left.\left.\left. + \delta p_{2i_2-1} + \sum_{k=1;k\neq i_1,i_2}^m \varrho_{2k-1}\delta p_{2k-1} + \sum_{k'=1}^n \varrho_{2k'}\delta p_{2k'}\right)^2\right\rangle\right.$$
$$< 1, \tag{36}$$

$$Y_3 = V_{2j_1,2j_2}^G = \langle(\delta x_{2j_1} - \delta x_{2j_2})^2\rangle + \left\langle\left(\left(\delta p_{2j_1} + \delta p_{2j_2}\right.\right.\right.$$
$$\left.\left.\left. + \sum_{k=1}^m \chi_{2k-1}\delta p_{2k-1} + \sum_{k'=1;k'\neq j_1,j_2}^n \chi_{2k'}\delta p_{2k'}\right)^2\right\rangle\right.$$
$$< 1. \tag{37}$$

The superscript G designates the GHZ state, $i,i_1,i_2,k = 1,2,\ldots,m$ ($i_1 \neq i_2$), and $j,j_1,j_2,k' = 1,2,\ldots,n$ ($j_1 \neq j_2$). $f_{2k'(2k-1)}, \varrho_{2k'(2k-1)}$, and $\chi_{2k'(2k-1)}$ are arbitrary real parameters that are used to optimize the above inequalities, respectively. We consider the same case as in the preceding section [Eq. (30)]. When $m \geqslant 2$ and $n \geqslant 2$, calculating the minimum values of the expressions in Eq. (35), we obtain the following optimization parameters:

$$f_1 = f_{2k-1} = u_1/u, \quad f_2 = f_{2k'} = u_2/u, \tag{38}$$

with

$$u = mn(x^2-1)^2 + 8(m+n-2)x^2,$$
$$u_1 = 16(n-1)x^2 - 8nx^2 + 4\sqrt{mn}(x^3+x), \tag{39}$$
$$u_2 = 16(m-1)x^2 - 8mx^2 + 4\sqrt{mn}(x^3+x).$$

In the same way, for Eq. (36), we have

$$\varrho_1 = \varrho_{2k-1} = b_1/b, \quad \varrho_2 = \varrho_{2k'} = b_2/b, \qquad (40)$$

with

$$b = x^2/m + (x^2 - 1)^2/16,$$
$$b_1 = x^2/m, \quad b_2 = x(x^2 + 1)/\sqrt{4mn}, \qquad (41)$$

and for Eq. (37), we have

$$\chi_1 = \chi_{2k-1} = d_1/d, \quad \chi_2 = \chi_{2k'} = d_2/d, \qquad (42)$$

with

$$d = x^2/n + (x^2 - 1)^2/16,$$
$$d_1 = x(x^2 + 1)/\sqrt{4mn}, \quad d_2 = x^2/n. \qquad (43)$$

Letting

$$\vartheta_1 = 1 + (m - 1)f_1, \quad \vartheta_2 = 1 + (n - 1)f_2,$$
$$\ell_1 = 2 + (m - 2)\varrho_1, \quad \ell_2 = n\varrho_2, \qquad (44)$$
$$J_1 = m\chi_1, \quad J_2 = 2 + (n - 2)\chi_2,$$

we obtain

$$
\begin{aligned}
Y_1(0) = {} & 1 + \frac{m-1}{4}f_1^2 + \frac{n-1}{4}f_2^2 \\
& + \left(\frac{1+\vartheta_1^2}{m} + \frac{1+\vartheta_2^2}{n}\right)\frac{2x^2}{(x^2-1)^2} \\
& - \frac{2(1+\vartheta_1\vartheta_2)}{\sqrt{mn}}\frac{x(x^2+1)}{(x^2-1)^2},
\end{aligned}
\qquad (45)
$$

$$
\begin{aligned}
Y_2(0) = {} & 1 + \frac{m-2}{4}\varrho_1^2 + \frac{n}{4}\varrho_2^2 + \left(\frac{\ell_1^2}{m} + \frac{\ell_2^2}{n}\right)\frac{2x^2}{(x^2-1)^2} \\
& - \frac{2\ell_1\ell_2}{\sqrt{mn}}\frac{x(x^2+1)}{(x^2-1)^2},
\end{aligned}
\qquad (46)
$$

$$
\begin{aligned}
Y_3(0) = {} & 1 + \frac{m}{4}\chi_1^2 + \frac{n-2}{4}\chi_2^2 + \left(\frac{J_1^2}{m} + \frac{J_2^2}{n}\right)\frac{2x^2}{(x^2-1)^2} \\
& - \frac{2J_1J_2}{\sqrt{mn}}\frac{x(x^2+1)}{(x^2-1)^2}.
\end{aligned}
\qquad (47)
$$

When $m = 1$ $(n = 1)$, there is no f_{2k-1} $(f_{2k'})$, i.e., no f_1 (f_2), and we can also use Eq. (45) to calculate the correlation $Y_1(0)$. When $m = 2$ $(n = 2)$, there is no ϱ_{2k-1} $(\chi_{2k'})$, i.e., no ϱ_1 (χ_2), and we can also use Eq. (46) [Eq. (47)] to calculate the correlation $Y_2(0)$ [$Y_3(0)$]. Next, we show numerical results of $Y_{1,2,3}(0)$ for detecting CV GHZ entanglement.

In Fig. 5, we present the output zero-frequency spectra $Y_1(0)$ as functions of x for different mode numbers m and n. It is easy to see that each curve of $m = n$ has one deep valley and is less than 1 for $x > 0$. When $m < n$, the spectra bifurcate close to $x = 1$, but all of them are smaller than 1 over a wide region of $x \neq 1$.

Recall that up to local Fourier transforms, the cluster state of $m = 1$ is equivalent to a GHZ-type state [23,44]. Also we can see that Figs. 4(a) and 5(a) are exactly the same, i.e., for $m = 1$, $Y_C(0) = Y_1(0)$. When $m = 1$ and $n \geqslant 2$, there are GHZ-type clusters [23,44]: linear three-mode, cross-shaped,
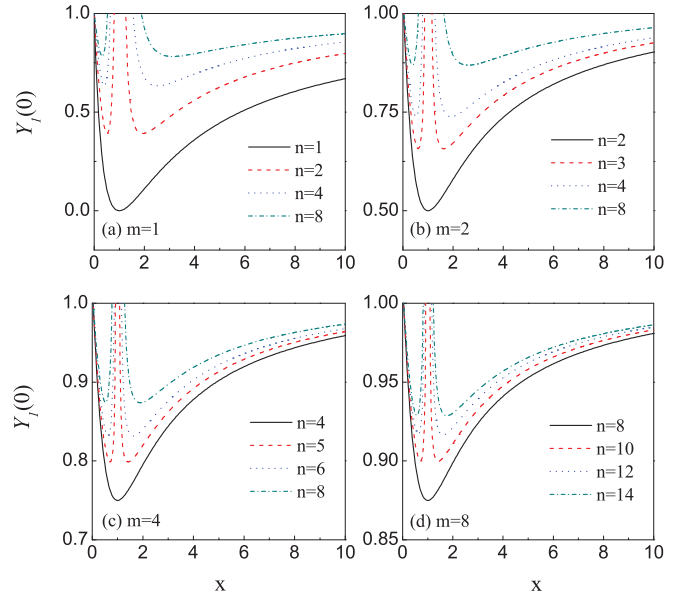

FIG. 5. (Color online) The (dimensionless) output zero-frequency spectra $Y_1(0)$ as functions of x (dimensionless) for different mode numbers m,n.

and star-shaped clusters, as shown in Figs. 3(i)–3(iii), respectively. When $m \geqslant 2$, cluster entanglement is different from GHZ entanglement, as demonstrated in Figs. 4(b)–4(d) and Figs. 5(b)–5(d).

Figure 6 depicts the correlations $Y_2(0)$ and $Y_3(0)$. First, we examine the case of $m = n$ and find $Y_2(0) = Y_3(0)$, as indicated in Fig. 6(a). With the increasing of m and n, the curves arise. As for $m < n$, we have $Y_2(0) < Y_3(0)$. Some examples are shown in Figs. 6(b)–6(d). We can see that all the curves are below 1 except $x = 0$. Thus all the inequalities in Eqs. (35)–(37) can be simultaneously satisfied, and hence the full inseparability of the created GHZ entangled states is verified [43]. Possible GHZ states are
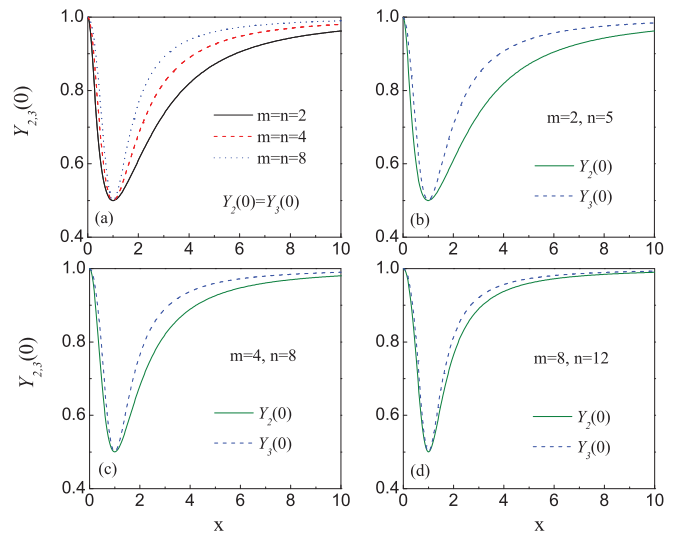

FIG. 6. (Color online) The (dimensionless) output zero-frequency spectra $Y_{2,3}(0)$ as functions of x (dimensionless) for different mode numbers m,n.
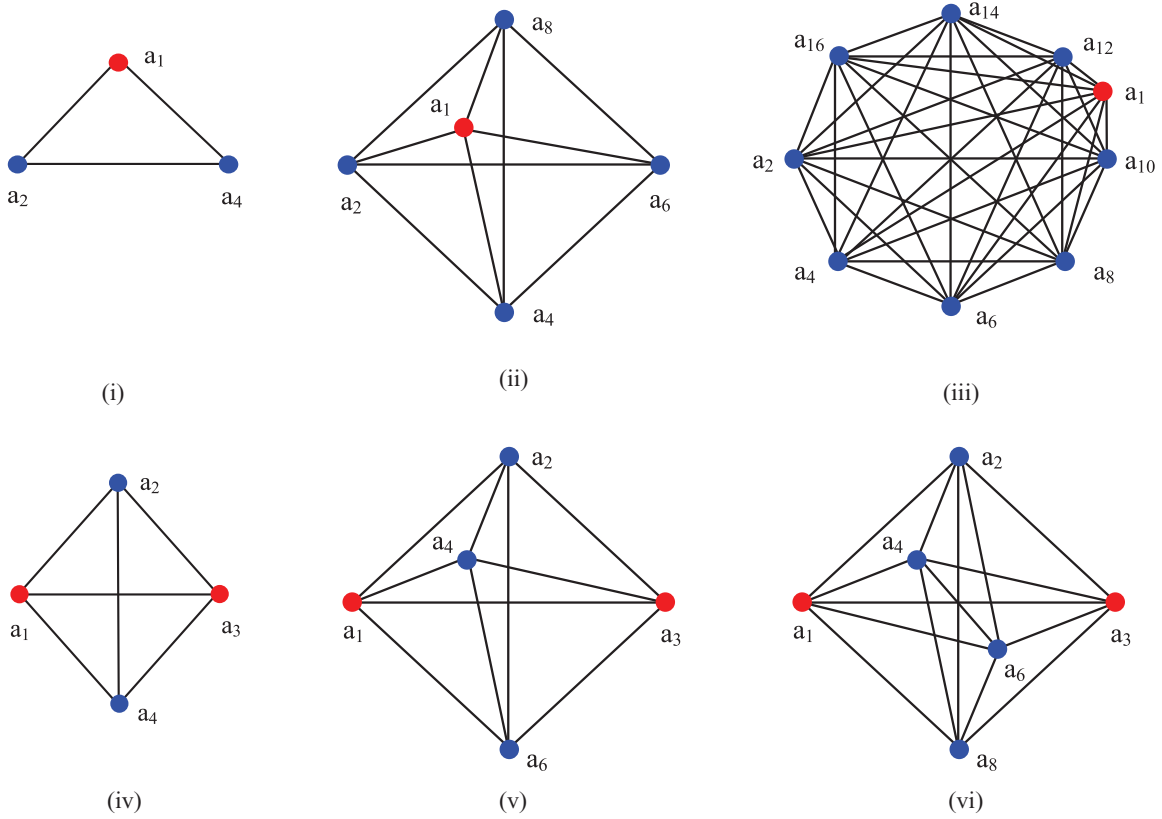
FIG. 7. (Color online) Possible GHZ states for different numbers of red sidebands a_{2i-1} and blue sidebands a_{2j}, $i = 1 \sim m$ and $j = 1 \sim n$. For $m = 1$, (i) $n = 2$, (ii) $n = 4$, and (iii) $n = 8$. For $m = 2$, (iv) $n = 2$, (v) $n = 3$, (vi) $n = 4$. Each vertex takes the role of one mode, and edges represent the interactions between the connected vertices.

exemplified in Fig. 7. Note that the star graphs for different central vertices as well as the complete graph are local Clifford (LC) equivalent representations of the GHZ state [17]. Thus Figs. 3(i)–3(iii) are LC equivalent to Figs. 7(i)–7(iii), respectively [45].

These results are due to the multiple four-photon processes in the large detuning limit (Fig. 1): In every transition channel, two photons are absorbed from the corresponding driving field, and then two sideband photons are emitted into the cavity fields. The sideband photons are simultaneously generated and highly correlated. The driving fields not only induce the above process but also create the coherence between the excited states. Due to the coherence, the atom-driving-field interactions are reduced to the $|0\rangle - |\tilde{1}\rangle$ transition. The atomic superposition states $|\tilde{j}\rangle$ are empty, i.e., $\langle \sigma_{\tilde{j}\tilde{j}} \rangle = 0$, $j = 2, 3, \ldots, n$. The cavity fields as collective fields A_1 and A_2 interact with the dressed transition of the $|0\rangle - |\tilde{1}\rangle$ transition. In the mean time, the collective modes A_{2i-1} and A_{2j} $(i, j \geqslant 2)$ remain at the vacuum states. This establishes the quantum beats between the cavity fields [31–34]. Taking the inverse of the transformations in Eq. (6), we obtain the beat signals as $\langle a_{2k-1}^\dagger a_{2l-1} \rangle = \tilde{U}_{1k}^m \tilde{U}_{1l}^m \langle A_1^\dagger A_1 \rangle$ $(k, l = 1, 2, \ldots, m, \ k \neq l)$ and $\langle a_{2k}^\dagger a_{2l} \rangle = \bar{U}_{1k}^n \bar{U}_{1l}^n \langle A_2^\dagger A_2 \rangle$ $(k, l = 1, 2, \ldots, n, k \neq l)$. In the presence of the quantum beats, all the higher sidebands behave collectively, and so do the lower sidebands. It is through collective modes A_1 and A_2 that all the cavity modes interact with the dressed atoms. By such a mechanism, the two-photon correlations are established. In a word, the quantum beats

and the wave-mixing interactions combine to induce the multipartite inseparability.

Alkali atomic systems fit in this scheme. We use an ensemble of cold atoms to avoid the Doppler effect and resolve the fine levels. We give two examples for the experimental realization of the present scheme. The first example is for the $m = n = 3$ case. We can use the Zeeman sublevels $(m_j = 0, \pm 1)$ of the excited state $^1P_1$. The transition $^1P_1 \to {}^1S_0$ is split into three by using a magnetic field. The corresponding resonance frequencies are far from each other when the magnetic field is relatively strong. The other example is for the $m = n = 4$ scheme. We can use the D_1 (794.8 nm) and D_2 (780.0 nm) transitions of the rubidium atom. The corresponding states are $|0\rangle = |5S_{1/2}, F = 2\rangle$, $|1\rangle = |5P_{1/2}, F' = 1\rangle$, $|2\rangle = |5P_{1/2}, F' = 2\rangle$, $|3\rangle = |5P_{3/2}, F'' = 2\rangle$, and $|4\rangle = |5P_{3/2}, F'' = 3\rangle$, respectively. The adjacent excited state $|5P_{3/2}, F'' = 1\rangle$ is below $|3\rangle$ by 157 MHz. So the nonresonant hyperfine interactions of the applied fields with adjacent transitions can be avoided. Since $|5S_{1/2}, F = 1\rangle$ is below $|5S_{1/2}, F = 2\rangle$ by 6.8 GHz, we can use the transition $|5S_{1/2}, F = 1\rangle - |5P_{3/2}, F = 0\rangle$ as a repumping transition.

VI. CONCLUSION

In this paper, we have presented an approach to generating unitarily multimode squeeze operators and CV multipartite cluster and GHZ entangled states. Through a suitable laser system, we are able to engineer a squeeze field operator

decoupled from the atomic degrees of freedom, yielding a large squeeze parameter that is proportional to the number of atoms. The physical mechanism is attributed to the multiple four-photon processes and the dispersive atom-cavity-field interaction in large detuning systems.

[1] R. Loudon and P. L. Knight, J. Mod. Opt. **34**, 709 (1987).

[2] V. V. Dodonov, J. Opt. B: Quantum Semiclass. Opt. **4**, R1 (2002).

[3] D. F. Walls, Nature (London) **306**, 141 (1983); D. F. Walls and G. J. Milburn, *Quantum Optics* (Springer, Berlin, 1994).

[4] C. M. Caves, K. S. Thorne, R. W. P. Drever, V. D. Sandberg, and M. Zimmermann, Rev. Mod. Phys. **52**, 341 (1980).

[5] S. L. Braunstein and P. van Loock, Rev. Mod. Phys. **77**, 513 (2005); *Quantum Information with Continuous Variables*, edited by S. L. Braunstein and A. K. Pati (Kluwer, Dordrecht, 2003).

[6] D. Wilson, J. Lee, and M. S. Kim, J. Mod. Opt. **50**, 1809 (2003).

[7] H. Jeong, J. Lee, and M. S. Kim, Phys. Rev. A **61**, 052101 (2000).

[8] Fan Hong-yi and Fan Yue, Phys. Rev. A **54**, 958 (1996); X. Liang, X. M. Hu, and C. He, *ibid.* **85**, 032329 (2012).

[9] S. Lloyd and S. L. Braunstein, Phys. Rev. Lett. **82**, 1784 (1999).

[10] S. Olivares, Eur. Phys. J. Spec. Top. **203**, 3 (2012).

[11] A. Ferraro, S. Olivares, and M. G. A. Paris, *Gaussian States in Quantum Information* (Bibliopolis, Naples, 2005).

[12] X.-B. Wang, T. Hiroshima, A. Tomita, and M. Hayashi, Phys. Rep. **448**, 1 (2007).

[13] G. Adesso and S. Piano, Phys. Rev. Lett. **112**, 010401 (2014); G. Adesso and F. Illuminati, J. Phys. A **40**, 7821 (2007).

[14] C. Weedbrook, S. Pirandola, R. Garcia-Patron, N. J. Cerf, T. C. Ralph, J. H. Shapiro, and S. Lloyd, Rev. Mod. Phys. **84**, 621 (2012).

[15] *Quantum Information with Continuous Variables of Atoms and Light*, edited by N. Cerf, G. Leuchs, and E. S. Polzik (Imperial College Press, London, 2007).

[16] M. Hein, J. Eisert, and H. J. Briegel, Phys. Rev. A **69**, 062311 (2004).

[17] M. Hein, W. Dür, J. Eisert, R. Raussendorf, M. Van den Nest, and H. J. Briegel, in *Quantum Computer, Algorithms and Chaos*, Proceedings of the International School of Physics "Enrico Fermi", edited by G. Casati, D. L. Shepelyansky, P. Zoller, and G. Benenti, Vol. 162 (IOS, Amsterdam, 2006); see also arXiv:quant-ph/0602096.

[18] J. Zhang and S. L. Braunstein, Phys. Rev. A **73**, 032318 (2006); J. Zhang, *ibid.* **78**, 034301 (2008).

[19] N. C. Menicucci, S. T. Flammia, and P. van Loock, Phys. Rev. A **83**, 042335 (2011).

[20] H. J. Briegel and R. Raussendorf, Phys. Rev. Lett. **86**, 910 (2001).

[21] R. Raussendorf and H. J. Briegel, Phys. Rev. Lett. **86**, 5188 (2001).

[22] N. C. Menicucci, S. T. Flammia, H. Zaidi, and O. Pfister, Phys. Rev. A **76**, 010302(R) (2007).

[23] P. van Loock, C. Weedbrook, and M. Gu, Phys. Rev. A **76**, 032321 (2007).

[24] X. Su, A. Tan, X. Jia, J. Zhang, C. Xie, and K. Peng, Phys. Rev. Lett. **98**, 070502 (2007).

[25] R. Guzmán, J. C. Retamal, E. Solano, and N. Zagury, Phys. Rev. Lett. **96**, 010502 (2006).

[26] H. Sun and X. M. Hu, J. Phys. B **44**, 205504 (2011).

[27] P. Meystre and M. Sargent, III, *Elements of Quantum Optics* (Springer, Berlin, 1991).

[28] R. W. Boyd, *Nonlinear Optics* (Academic, New York, 1992).

[29] M. Ikram, G. X. Li, and M. S. Zubairy, Phys. Rev. A **76**, 042317 (2007).

[30] S. Pielawa, G. Morigi, D. Vitali, and L. Davidovich, Phys. Rev. Lett. **98**, 240401 (2007).

[31] M. O. Scully, Phys. Rev. Lett. **55**, 2802 (1985).

[32] M. P. Winters, J. L. Hall, and P. E. Toschek, Phys. Rev. Lett. **65**, 3116 (1990).

[33] J. A. Bergou, M. Orszag, and M. O. Scully, Phys. Rev. A **38**, 754 (1988); N. Lu, *ibid.* **45**, 8154 (1992).

[34] X. M. Hu and J. H. Zou, Phys. Rev. A **78**, 045801 (2008); X. X. Li and X. M. Hu, *ibid.* **80**, 023815 (2009).

[35] C. Cohen-Tannoudji, J. Dupont-Roc, and G. Grynberg, *Atom-Photon Interactions* (Wiley, New York, 1992).

[36] D. F. V. James, Fortschr. Phys. **48**, 823 (2000).

[37] C. W. Gardiner and P. Zoller, *Quantum Noise* (Springer, Berlin, 2000).

[38] C. M. Caves and B. L. Schumaker, Phys. Rev. A **31**, 3068 (1985).

[39] C. F. Lo and R. Sollie, Phys. Rev. A **47**, 733 (1993).

[40] M. Gu, C. Weedbrook, N. C. Menicucci, T. C. Ralph, and P. van Loock, Phys. Rev. A **79**, 062318 (2009).

[41] W. Dür, H. Aschauer, and H. J. Briegel, Phys. Rev. Lett. **91**, 107903 (2003).

[42] H. Aschauer, W. Dür, and H. J. Briegel, Phys. Rev. A **71**, 012319 (2005); W. Dür, J. Calsamiglia, and H. J. Briegel, *ibid.* **71**, 042336 (2005).

[43] P. van Loock and A. Furusawa, Phys. Rev. A **67**, 052315 (2003).

[44] P. van Loock and S. L. Braunstein, Phys. Rev. Lett. **84**, 3482 (2000).

[45] O. Gühne, G. Tóth, P. Hyllus, and H. J. Briegel, Phys. Rev. Lett. **95**, 120405 (2005).